

Geometrical aspects of protein folding

JAYANTH R. BANAVAR¹, AMOS MARITAN², CRISTIAN MICHELETTI² & FLAVIO SENO³

¹ Department of Physics and Center for Materials Physics, 104 Davey Laboratory, The Pennsylvania State University, University Park, Pennsylvania 16802, USA

² International School for Advanced Studies (S.I.S.S.A.), Via Beirut 2-4, 34014 Trieste, Istituto Nazionale per la Fisica della Materia and the Abdus Salam International Center for Theoretical Physics, Trieste, Italy

³ Istituto Nazionale per la Fisica della Materia (INFN) and Dipartimento di Fisica G.Galilei, via Marzolo 8, 35131 Padova , Italy

1. – Scope of the lectures

These lectures will address two questions. Is there a simple variational principle underlying the existence of secondary motifs in the native state of proteins? Is there a general approach which can qualitatively capture the salient features of the folding process and which may be useful for interpreting and guiding experiments? Here, we present three different approaches to the first question, which demonstrate the key role played by the topology of the native state of proteins. The second question pertaining to the folding dynamics of proteins remains a challenging problem – a detailed description capturing the interactions between amino acids among each other and with the solvent is a daunting task. We address this issue building on the lessons learned in tackling the first question and apply the resulting method to the folding of various proteins including HIV protease and membrane proteins. The results that will be presented open a fascinating perspective: the two questions appear to be intimately related. The variety of results reported here all provide evidence in favour of the special criteria adopted by nature in the selection of viable protein folds, ranging from optimal compactness to maximum dynamical and geometrical accessibility of the native states.

Acknowledgments. We are indebted to Fabio Cecconi, Alessandro Laio, Enzo Orlandi

dini, Gianni Settanni and Antonio Trovato who have contributed to the results discussed in these lectures.

2. – Introduction

A fascinating and open question challenging biochemistry, physics and even geometry is the presence of highly regular motifs such as α -helices and β -sheets in the folded state of biopolymers and proteins. Stimulating explanations ranging from chemical propensity to simple geometrical reasoning have been invoked to rationalize the existence of such secondary structures.

The realization that proteins have secondary structures arose with early crystallographic studies and the brilliant deduction of Pauling et al. [1] of the ability of an α -helix of the correct pitch to accommodate hydrogen bonds, thus promoting its stability. Inspired by the findings of Pauling, helix-coil transition models have been used to study the thermodynamics of helix formation [2]. It is interesting to note, however, that the number of hydrogen bonds is nearly the same when a sequence is in an unfolded structure in the presence of a polar solvent or in its native state rich in secondary structure content [3]. It has also been suggested that the α -helix is an energetically favorable conformation for main-chain atoms but the side-chain suffers from a loss of entropy [3, 4]. Nelson *et al.* [5] have shown both numerically and experimentally that non-biological oligomers fold reversibly like proteins into a specific three-dimensional structure with high helical content driven only by solvophobic interactions.

Recent studies have attempted to explain the emergence of secondary structure in proteins from geometrical principles rather than invoking detailed chemistry. Despite the concerted efforts of several groups, a simple general explanation remains elusive. A very natural line of investigation was undertaken by Yee *et al.* [6], Hunt *et al.* [3], and Socci *et al.* [7] who focused on the spontaneous emergence of secondary content from the mere requirement of overall compactness of homopolymeric chains. Their findings ruled out any significant relationship between the two, a fact also corroborated by the recent study of the kinetics of homopolymer collapse, where no evidence was found for the formation of local regular structures [8]. Despite the failure, this approach is particularly interesting due to the fact that optimal packing is a fundamental and fascinating problem in contexts ranging from every day like to atomic physics. Perhaps, the best known packing problem is the one introduced by Kepler nearly four centuries ago, concerning the optimal packing of sphere. However the packing of independent objects, like spheres, must be treated differently from the case of objects connected in a chain, such as beads in a string (an idealization of peptide chains). In Sec. **3**, the packing problem is generalized to such chains and, remarkably, if one requires optimal packing uniformly along the chain, then a particular type of helix becomes the solution and, furthermore, it has the same geometrical characteristics as α -helices found in proteins.

In addition to packing considerations, dynamical effects also play a significant role when rapid packing/unpacking is entailed, as in the formation of amorphous glasses where crystallization is dynamically thwarted or in the more familiar problem of packing clothes

in one's suitcase. The same question may be asked for protein-like structure. The fact that they contain motifs which are optimally compact, does not imply that they can be easily reached from unfolded states. It is, however, widely believed that native states are, in general, highly accessible from the kinetic point of view. To investigate this issue we formulate, in Sec. 4, a dynamical variational principle for selection in conformation space based on the requirement that the backbone of the native state of biologically viable polymers be rapidly accessible from the denatured state. The variational principle is shown to result in the emergence of helical order in compact structures, revealing a surprising accord with the compactness requirement discussed above.

Still concerning the folding dynamics, there are two key aspects distinguishing a protein from a generic heteropolymer: the specially selected sequence of amino acids and the three-dimensional structure that it folds reversibly into. Nature uses a rich repertoire of twenty kinds of amino acids with sometimes major and at other times subtle differences in their interactions with the solvent and with each other in order to design sequences that fit the putative native state with minimal frustration [9]. The chosen sequences are such that their target native states are reached through a funnel-like landscape [10, 11, 12, 13] which facilitates the harmonious fitting together of pieces to form the whole. The three-dimensional structure impacts on the functionality of the protein and a fascinating issue is the elucidation of the selection mechanism in conformation space that picks out certain viable structures from the innumerable ones with a given compactness. Earlier studies have shown that there is a direct link between viable native conformations and high designability [14, 15].

A fruitful and general strategy for the study of protein folding would be to extract information on the folding process directly from the topology of the native state. This problem will be elucidated in Sec. 5 and applied to HIV protease and in Sec. 6 to membrane proteins. It will be shown that the natural folds of proteins have a much larger density of nearby structures than generic (artificial) conformations of the same character and that the exceedingly large geometrical accessibility of natural proteins may be related to the presence of secondary motifs [16]. It will be shown that a study of the influence of native state topology on the folding process can reveal information about the sites that are crucial to the folding process itself. As an application, we shall identify such sites for three proteins: 2ci2, barnase and HIV-1 Protease and show that they correlate very well with the key folding sites identified in experiments.

In Sec. 6, a general model based on topological properties of the native state is introduced to decipher the folding of membrane proteins. Nearly a quarter of genomic sequences and almost half of all receptors that are likely to be targets for drug design [17] are integral membrane proteins. Understanding the detailed mechanisms of their folding mechanism is a largely unsolved, key problem in structural biology. By using our geometrical approach we can investigate the equilibrium properties and the folding kinetics of a two helix bundle fragment (comprising 66 amino-acids) of Bacteriorhodopsin. Once again, the approach seems to be extremely powerful and it appears to provide an efficient framework for understanding the variety of folding pathways of transmembrane proteins.

3. – Optimal shape of a compact polymeric chain

A fundamental problem in every day life is that of packing with examples ranging from fruits in a grocery, clothes and personal belongings in a suitcase, atoms and colloidal particles in crystals and glasses, and amino acids in the folded state of proteins [18, 19, 20, 21, 22]. The simplest problem in packing consists of determining the spatial arrangement that accomodates the highest packing density of its constituent entities with the result being a crystalline structure.

A classic problem is the determination of the optimal arrangement of spheres in three dimensions in order to achieve the highest packing fraction. This problem first posed by Kepler has attracted much interest culminating in its recent rigorous mathematical solution [18, 19] that the answer for infinite systems is a face-centred-cubic lattice. This simply stated problem has had a profound impact in many areas [20, 21, 22], ranging from the crystallization and melting of atomic systems, to optimal packing of objects and subdivision of space.

The close-packed hard sphere problem is simply stated: given N hard spheres of radius R , what is the arrangement which can be enclosed in the minimum volume, e.g. a cube of side L . This is solved by reformulating the problem, more convenient for numerical implementation, as the determination of the arrangement of a set of N points in a cube of linear size, L_0 , that results in the minimum of half the distance between any pair of points or between the points and walls of the container, denoted by r_{min} , being as large as possible [23]. The linear size associated with the region enclosing the hard spheres follows from dimensional analysis and it is given by $L = RL_0/r_{min}$, from which it follows that maximizing r_{min} is equivalent to minimizing L . It is notable that the resulting ‘bulk’ optimal arrangement in the large N limit exhibits translational invariance in that, far from the boundaries, the local environment is the same for all points. In dimension $d = 2$ and $d = 3$ this corresponds to triangular and face-centred-cubic lattices respectively.

Biopolymers like proteins, DNA and RNA have three dimensional structures which are rather compact. Furthermore, they are the result of evolution and one may think that their shape may satisfy some optimality criterion. This naturally leads one to consider a generalization of the packing problem of hard spheres to the case of flexible tubes with a uniform cross section. The packing problem then consists in finding the tube configuration which can be enclosed in the minimum volume without violating any steric constraints.

The problem can alternatively be formulated in a very simple and elegant way in terms of the curve which is the axis of the tube (the analog of the sphere centers in the hard sphere packing problem) [24]. Consider a string (an open curve) in three dimensions. We will utilize a geometric measure [25] of the curve, the ‘rope-length’, defined as the arc length measured in units of the thickness, which has proved to be valuable in applications of knot theory [25, 26, 27, 28, 29, 30]. The thickness Δ denotes the maximum radius of a uniform tube with the string passing through its axis, beyond which the tube either ceases to be smooth, owing to tight local bends, or it self-intersects. Our focus is on finding the optimal shape of a curve of fixed arc length, subject to constraints of compactness,

which would maximize its thickness, or equivalently minimize its rope length.

Following the approach of Gonzalez and Maddocks [28], who studied knotted strings, we define a global radius of curvature as follows. The global radius of curvature of the curve at a given point is computed as the minimum radius of the circles going through that point and all other pairs of points of the string. It generalizes the concept of the local radius of curvature (the radius of the circle which locally best approximates the curve) by taking into account both local (bending of the string) and non-local (proximity to another part of the string) effects. For discretized curves, the local radius of curvature at a point is simply the radius of the circle going through the point and its two adjoining points. The minimum of all the global radii then defines the thickness, i.e. the minimum radius of the circles going through any triplet of discrete points. This coincides with the previous definition in the continuum limit, obtained on increasing the number of discretized points (assumed to be equally spaced) on the curve keeping the string length fixed [28]. Given a string configuration, the thickness is just the maximum allowed radius for the cross section of a uniform tube that has the given curve as its axis [28].

We used several different boundary conditions to enforce the confinement of the string. The simplest ones discussed here are the confinement of a curve of length l within a cube of side L or constraining it to have a radius of gyration (which is the root-mean-square distance of the discretized points from their centre of mass) that is less than a pre-assigned value R . Even though different boundary conditions influence the optimal string shape, the overall features are found to be robust. Examples of optimal shapes, obtained from numerical simulations, for different ratios of l/L and l/R are shown in Fig. 1. In both cases, two distinct families of curves, helices and saddles, appear. The two families are close competitors for optimality and different boundary conditions may stabilize one over the other. For example, if optimal strings of fixed length are constrained to have a radius of gyration less than R , then upon decreasing R , the curve goes from a regime where the trivial linear string is curled into an arc, then into a portion of helix and finally into a saddle. When the string is constrained to lie within a cube of size L , as L decreases first saddles are observed and then helices.

We have also been able to find bulk-like solutions which are not influenced by boundary effects. Such solutions can be obtained by imposing uniform local constraints along the curve. On imposing a minimum local density on successive segments of the string (for example, constraining each set of six consecutive beads to have a radius of gyration that is less than a preassigned value R), we obtained perfectly helical strings, corresponding to discretised approximations to the continuous helix represented in Fig. 2 confirming that this is the optimal arrangement. Note that, in close analogy with the sphere-packing problem, a helix has translational invariance along the chain.

In all cases, the geometry of the chosen helix is such that there is an equality of the local radius of curvature (determined by the local bending of the curve) and the radius associated with a suitable triplet of non-consecutive points lying in two successive turns of the helix. This is a feature that is observed only for a special ratio c^* of the pitch, p , and the radius, r , of the circle projected by the helix on a plane perpendicular to its axis. When $p/r > c^* = 2.512$ the local radius of curvature, given by $\rho = r(1 + p^2/(2\pi r)^2)$,

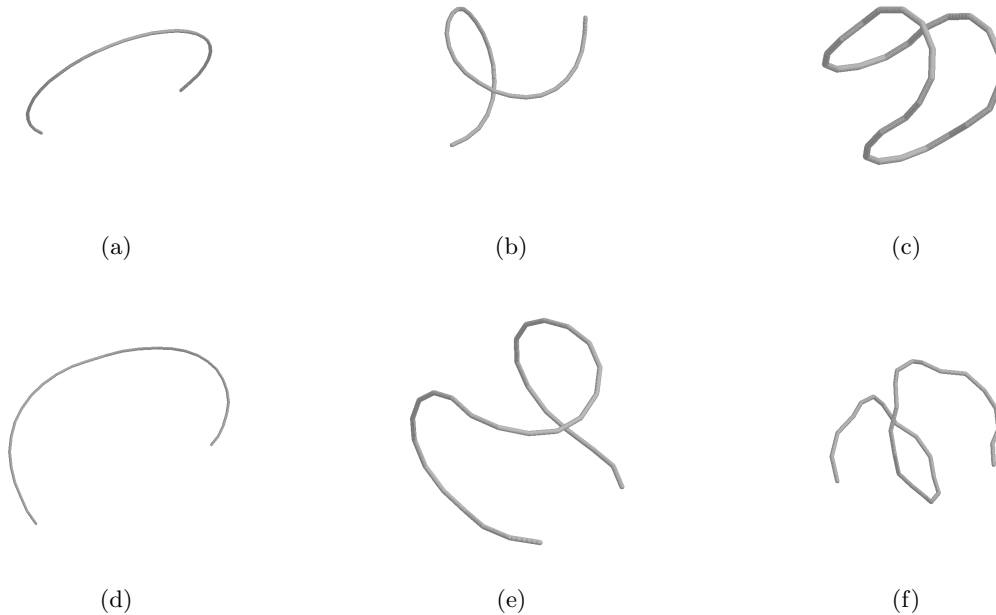


Fig. 1. – Examples of optimal strings. The strings in the figure were obtained starting from a random conformation of a chain made up of N equally spaced points (the spacing between neighboring points is defined to be 1 unit) and successively distorting the chain with pivot, crankshaft and slithering moves commonly used in stochastic chain dynamics [96]. A Metropolis Monte Carlo procedure is employed with a thermal weight, $e^{+\Delta/T}$, where Δ is the thickness and T is a fictitious temperature set initially to a high value such that the acceptance rate is close to 1 and then decreased gradually to zero in several thousand steps. Self-avoidance of the optimal string is a natural consequence of the maximization of the thickness. The introduction of a hard-core repulsion between beads was found to significantly speed up convergence to the optimal solution and avoid trapping in self-intersecting structures. We have verified that the same values (within 1 percent) of the final thickness of the optimal strings are obtained starting from unrelated initial conformations. Top row: optimal shapes obtained by constraining strings of 30 points with a radius of gyration less than R . (a) $R = 6.0$, $\Delta = 6.42$ (b) $R = 4.5$, $\Delta = 3.82$ (c) $R = 3.0$, $\Delta = 1.93$. Bottom row: optimal shapes obtained by confining a string of 30 points within a cube of side L . (d) $L = 22.0$, $\Delta = 6.11$ (e) $L = 9.5$, $\Delta = 2.3$ (f) $L = 8.1$, $\Delta = 1.75$.

is lower than the half of the distance of closest approach of points on successive turns of the helix. The latter is given by the first minimum of $1/2\sqrt{2 - 2\cos(2\pi t) + p^2 t^2}$ for $t > 0$. Thus $\Delta = \rho$ in this case.

If $p/r < c^*$, the global radius of curvature is strictly lower than the local radius, and the helix thickness is determined basically by the distance between two consecutive helix turns: $\Delta \simeq p/2$ if $p/r \ll 1$. Optimal packing selects the very special helices corresponding to the transition between the two regimes described above. A visual example is provided

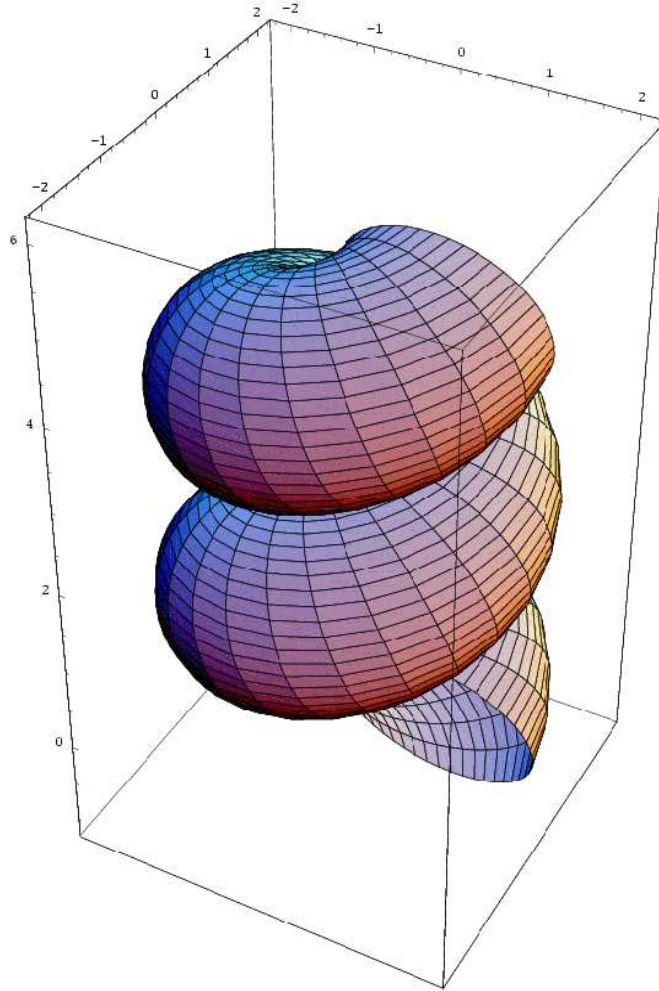


Fig. 2. – Shape of the optimal helix. The ratio of the pitch to radius of the centerline is 2.512.

by the optimal helix of Fig. 2.

For discrete curves, the critical ratio p/r depends on the discretization level. A more robust quantity is the ratio f of the minimum radius of the circles going through a given point and any two non-adjacent points and the local radius. For discretized strings, $f = 1$ just at the transition described above, whereas $f > 1$ in the ‘local’ regime and $f < 1$ in the ‘non-local’ regime. In our computer-generated optimal strings, f differed from unity by less than a part in a thousand.

It is interesting to note that, in nature, there are many instances of the appearance of

helices. For example, many biopolymers such, as proteins and enzymes, have backbones which frequently form helical motifs. (Rose and Seltzer [31] have used the local radii of curvature of the backbone as input in an algorithm for finding the peptide chain turns in a globular protein.) It has been shown [16] that the emergence of such motifs in proteins (unlike in random heteropolymers which, in the melt, have structures conforming to Gaussian statistics) is the result of the evolutionary pressure exerted by nature in the selection of native state structures that are able to house sequences of amino acids which fold reproducibly and rapidly [32] and are characterized by a high degree of thermodynamic stability [33]. Furthermore, because of the interaction of the amino acids with the solvent, globular proteins attain compact shapes in their folded states.

It is then natural to measure the shape of these helices and assess if they are optimal in the sense described here. The measure of f in α -helices found in naturally-occurring proteins yields an average value for f of 1.03 ± 0.01 , hinting that, despite the complex atomic chemistry associated with the hydrogen bond and the covalent bonds along the backbone, helices in proteins satisfy optimal packing constraints. An example is provided in Fig. 3 where we report the value of f for a particularly long α -helix encountered in a heavily-investigated membrane protein, bacteriorhodopsin.

This result implies that the backbone sites in protein helices have an associated free volume distributed more uniformly than in any other conformation with the same density. This is consistent with the observation [16] that secondary structures in natural proteins have a much larger configurational entropy than other compact conformations. This uniformity in the free volume distribution seems to be an essential feature because the requirement of a maximum packing of backbone sites by itself does not lead to secondary structure formation [6, 7]. Furthermore, the same result also holds for the helices appearing in the collagen native state structure, which have a rather different geometry (in terms of local turn angles, residues per turn and pitch [34]) from average α -helices. In spite of these differences, we again obtained an average $f = 1.01 \pm 0.03$ (Fig. 4), very close to the optimal situation.

4. – Fast folding polymers and role of secondary motifs

Fast packing has been recognized as a central issue for biopolymers, such as proteins, since the early work of Levinthal [35]. The packing of strings as defined above and the slope of the optimal string we have found should also be kinetically very accessible. We postulate a direct connection between the dynamics of rapid folding and the emergence of secondary motifs in the native state conformations [32]. In fact, an intuitive approach to rapid and reproducible folding might be to create neat patterns of lower dimensional manifolds than the physical space and bend and curl them into the final folded state. For proteins, secondary structures such as α -helices and β -sheets are indeed patterns in

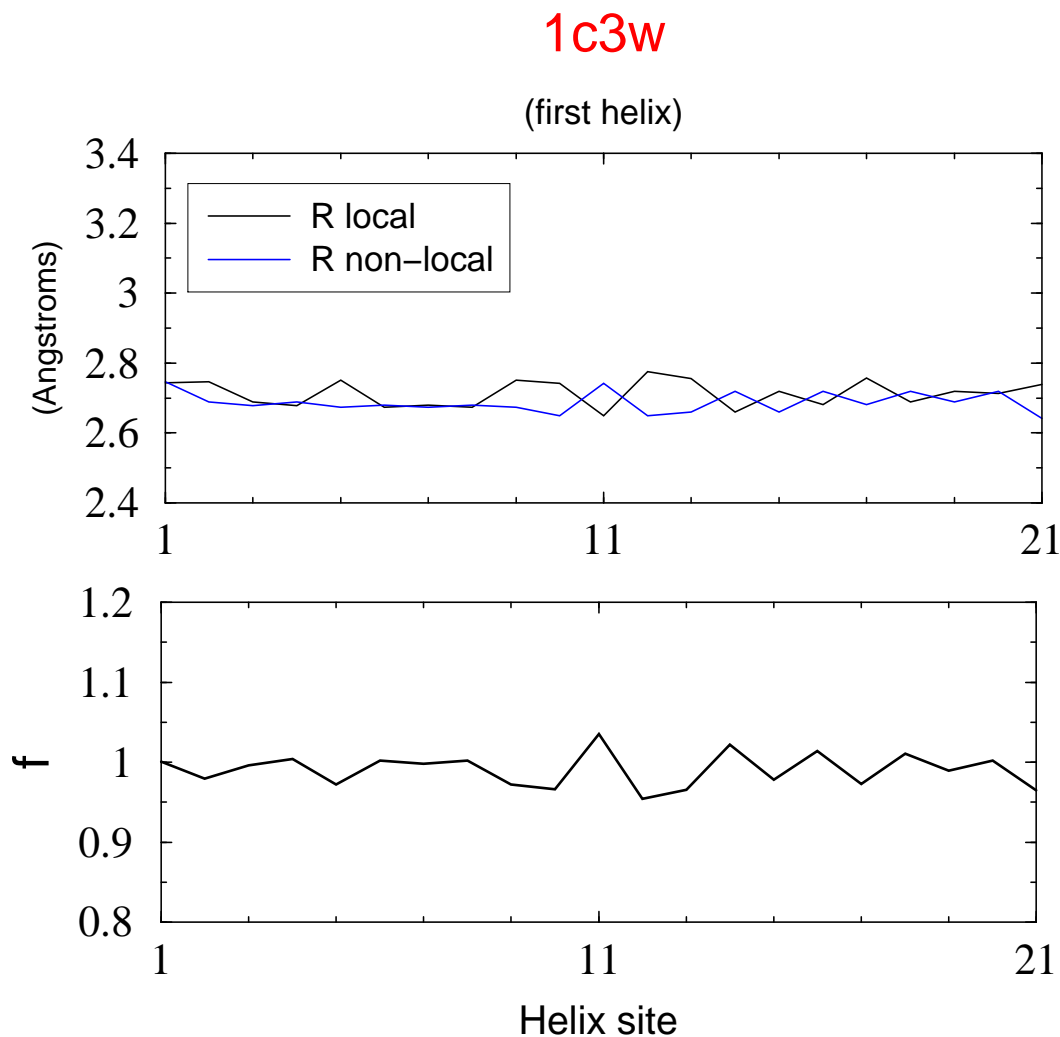


Fig. 3. – Top. Local and non-local radii of curvature for sites in the first helix of bacteriorhodopsin (pdb code 1c3w). Bottom. Plot of f values for the same sites.

low dimensions.

The selection mechanism in structure space is formulated as a variational principle postulating that, *among all possible native conformations, a protein backbone will attain only those which are optimal under the action of evolutionary pressure favouring rapid folding*. Our goal is to elucidate the role played by the bare native backbone independent of the selection in sequence space and hence of the (imperfectly-known) inter-amino-acid potentials. We therefore choose to employ a Go-like model [36] with no other interaction

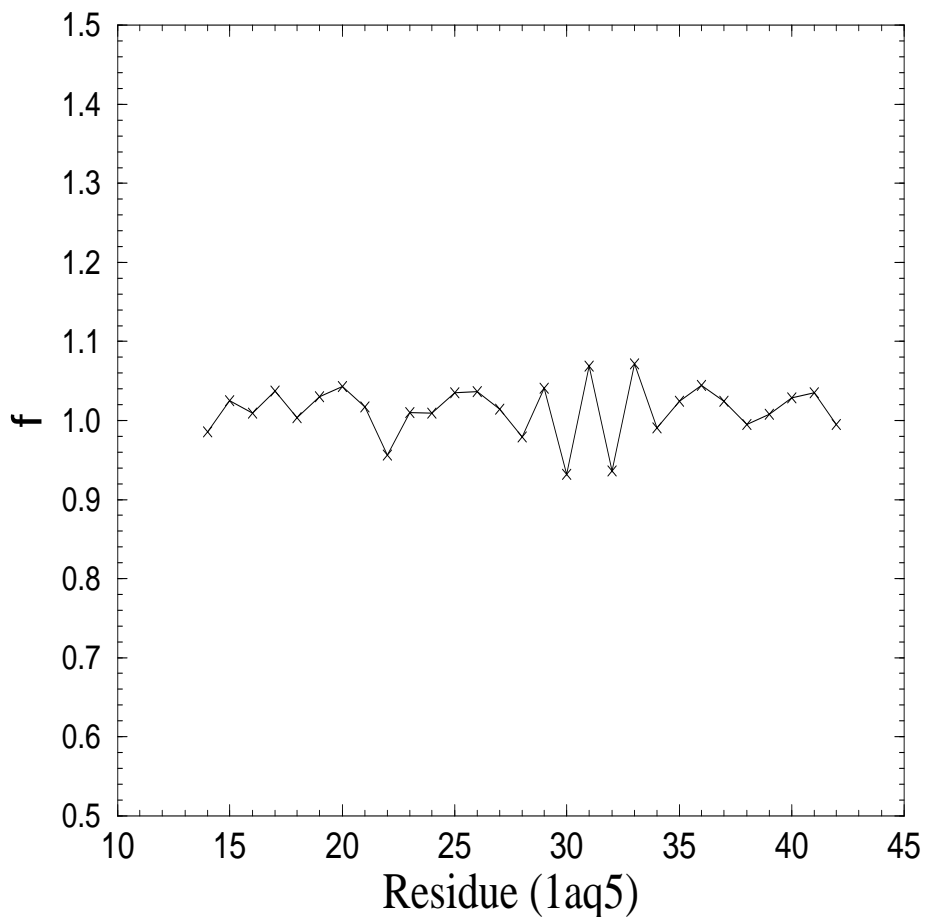


Fig. 4. – Packing of collagen helices. Plot of f values as a function of sequence position for a single collagen helix (only C_α coordinates were used to identify the protein backbone). The same plot for each of the three collagen chains would simply superimpose. We considered the residues 14-42 from the structure 1aq5 in the Protein Data Bank.

that promotes or disfavors secondary structures. The model is a sequence-independent limiting case of minimal frustration[9] which, for a given target native state conformation, favours the formation of native contacts – the energy of a sequence in a conformation is simply obtained as the negative of the number of contacts in common with the target conformation. We will work in the C_α representation and consider two non-consecutive amino acids to be in contact if their separation is below a cutoff $r_0 = 6.5 \text{ \AA}$ (the results are

qualitatively similar when slightly different values of r_0 in the range 6 – 8 Å are chosen). The energy of structure Γ in the Go model is given by

$$(1) \quad H(\Gamma) = -\frac{1}{2} \sum_{i,j} \Delta_{i,j}(\Gamma) \Delta_{i,j}(\Gamma_0)$$

where the sum is taken over all pairs of amino acids, Γ_0 is the target structure, $\Delta_{i,j}(\Gamma)$ is the contact map of structure Γ :

$$(2) \quad \Delta_{ij}(\Gamma) = \begin{cases} 1 & R_{ij} < r_0 \text{ and } |i - j| > 2; \\ 0 & \text{otherwise,} \end{cases}$$

where R_{ij} is the distance of amino acids i and j .

The polypeptide chain is modelled as a chain of beads subject to steric constraints [37, 16]. We adopted a discrete representation similar to the one of Covell and Jernigan [37, 38], in which each bead occupies a site of an FCC lattice with lattice spacing equal to 3.8 Å. Such a representation is able to describe the backbone of natural proteins to better than 1 Å rmsd per residue (equal to the best experimental resolution) and preserves typical torsional angles. All discretized structures were subject to a suitable constraint: any two non-consecutive residues cannot be closer than 4.65 Å due to excluded volume effects and the distance between consecutive residues can fluctuate between 2.6 Å $< d < 4.7$ Å. Such constraints were determined by an analysis of the coarse-grainings of several proteins of intermediate length (≈ 100 residues). In order to enforce a realistic global compactness for a backbone of length L , the number of contacts in all the target structures considered was chosen [39] to be around $N = 1.9L$ while, locally, no residue was allowed to make contact with four or more consecutive residues.

In order to assess the validity of the variational principle, it is necessary to evaluate the typical time, $t(\Gamma_0)$, taken to fold into a given target structure, Γ_0 , followed by a selection of the structures Γ_0 , that have the smallest folding times. To do this, an initial set of ten conformations was generated by collapsing a loose chain starting from random initial conditions. In each case, we modified the random initial conformation by using Monte Carlo dynamics: we move up to 3 consecutive beads to unoccupied discrete positions that do not violate any of the physical constraints and accept the moves according to the standard Metropolis rule. The energy is given by eq. (1), while the temperature for the MC dynamics was set to 0.35. This value was chosen in preliminary runs so that it was higher than the temperature [9] below which the sequence is trapped in metastable states but comparable to the folding transition temperature so that conformations with significant overlap with the native state are sampled in thermal equilibrium.

For each structure, as a measure of the folding time we took the median over various attempts (typically 41) of the total number of Monte Carlo moves necessary to form a pre-assigned fraction of native contacts, typically 66%, starting from a random conformation. Our results were unaltered on increasing this fraction to 75%; indeed, this fraction could

be progressively increased towards 100% with successive generations without increase in the computational cost since better and better folders are obtained.

A new generation of ten structures is created by “hybridizing” pairs of structures of the previous generation ensuring that structures with small folding times are hybridized more and more frequently as the number of generations, g , increases [40]. To do this, each of the two distinct parent structures to be paired, Γ_1 and Γ_2 are chosen with probability proportional to $\exp[-(g-1) * f_t/1000]$, where g is the index of the current generation (initially equal to 1), f_t is the median folding time. Then, a hybrid map is created by taking the union of the two parent maps:

$$(3) \quad \Delta_{ij}^{Union} = \max(\Delta_{ij}(\Gamma_1), \Delta_{ij}(\Gamma_2)) .$$

Because it is not guaranteed that Δ^{Union} corresponds to a three-dimensional structure obeying the same physical constraints as Γ_1 and Γ_2 , the corresponding hybrid Γ is constructed by taking one of the two parent structures (or alternatively a random one) as the starting conformation and carrying out MC dynamics favouring the formation of each of the contacts in the union map (i.e. using eq. (1) with $\Delta_{ij}(\Gamma_0)$ substituted by Δ_{ij}^{Union}). The dynamics is carried out starting from a temperature of 0.7 and then decreasing it gradually over a sufficiently long time (typically thousands of MC steps) to achieve the maximum possible overlap with the union map, while simultaneously maintaining the realistic compactness. The resulting structure is typically midway between the two parent structures, in that it inherits native contacts from both of them. We adopted the following definition in order to obtain an objective and unbiased way to quantitatively estimate the presence of secondary content: a given residue, i was defined to belong to a secondary motif if, for some j , one of these conditions held:

$$\begin{aligned} a) \quad \Delta_{i-1,j-1} &= \Delta_{i,j} = \Delta_{i+1,j+1} = \Delta_{i,j+1} \\ &= \Delta_{i+1,j+2} = \Delta_{i-1,j} = 1; \\ b) \quad \Delta_{i+1,j-1} &= \Delta_{i,j} = \Delta_{i-1,j+1} = \Delta_{i,j+1} \\ &= \Delta_{i+1,j} = \Delta_{i-1,j+2} = 1. \end{aligned}$$

The former [latter] identifies the presence of helices and parallel [anti-parallel] β sheets in natural proteins, which can be identified by the visual inspection of contact matrices and appears as thick bands parallel or orthogonal to the diagonal.

The upper plot of Fig. 5 shows the decrease of the typical folding time over the generations for chains of length 25, while the middle panel shows the accompanying increase in the number of residues in secondary motifs (secondary content). The bottom panel shows a milder decrease of the contact order (i.e. a larger number of short-range contacts) as the generations evolved, in agreement with the experimental findings of Plaxco *et al.*[41] One of the optimal structures of length 25 is shown in Figure 6a. Due to the absence of any chirality bias in our structure space exploration, the helix does not have a constant

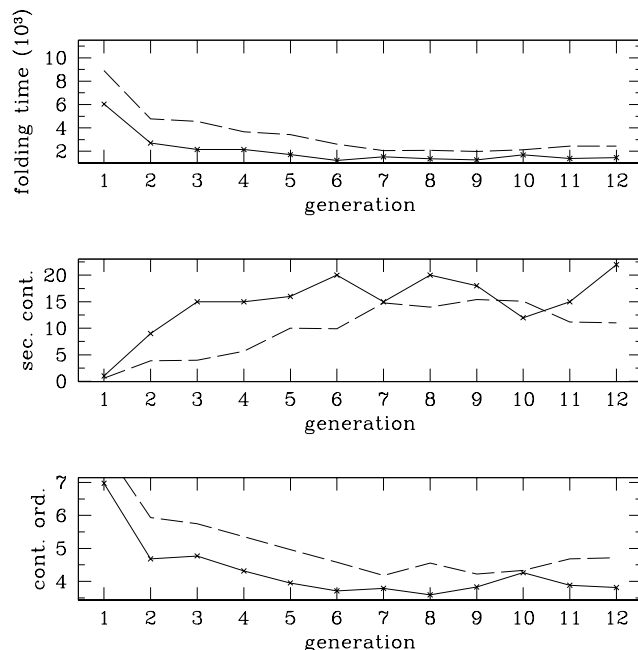


Fig. 5. – Evolution of the median folding time (measured in Monte Carlo steps), secondary structure content and contact order as a function of the number of generations in the optimization algorithm for compact structures of length $L = 25$. The dashed curve denotes an average over all ten structures in a given generation, whereas the solid curve shows the behaviour of the structure at each generation with the fastest median folding time. Analogous results are obtained for other runs and for other values of L . The dramatic decrease of folding time is accompanied by an equally significant increase in the secondary content.

handedness. The signature of the secondary motifs in the optimal structures is clearly visible in the contact maps of Figure 7, which are not sensitive to structure chirality. Strikingly, the variational principle selects conformations with significant secondary content as those facilitating the fastest folding. It is also noteworthy that the average value of f defined in Sec. 3 is 0.9, which is very close to the ideal value, $f = 1$, despite the fact that the underlying FCC lattice prevents the structures from attaining a regular helical shape.

The correlation of the emergence of secondary structures with decrease of folding times is shown in the plot of Fig. 8. We verified that the hybridization procedure is not biased towards low contact order by iterating it for various generations and pairing the structures at random. Even after dozens of generations, the generated structures had secondary contents of about 1/3-1/4 of the true extremal structures.

The very high secondary content in optimal conformations was found to be robust against changes in chain length or compactness of the target structure. On requiring that the

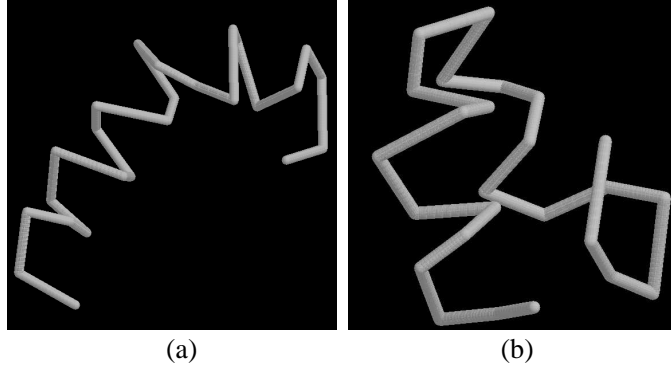


Fig. 6. – a) RASMOL plot of a structure with very low median folding time and $L = 25$. b) Structure with very low median folding time, $L = 25$ and higher compactness (all target conformations were constrained to have a radius of gyration smaller than 6.5 \AA). Optimal compact structures correspond to helices packed together, as observed in naturally occurring proteins.

structure be more compact, bundles of helices emerge [see Fig. 6b] along with an increase in contact order, signalling the presence of some longer range contacts, which are necessitated in order to accommodate the shorter radius of gyration. It is noteworthy that our calculations lead predominantly to α -helices and not β sheets, a fact accounted for by the demonstration that steric overlaps and the associated loss of entropy lead to the destabilization of helices in favor of sheets [4], the appearance of such sheets only in sufficiently long proteins[42] and the much slower folding rate of β -sheets compared to α -helices [43]. It is remarkable that the same requirement of rapid folding is sufficient to lead to a selection in both sequence and structure space underscoring the harmony in the evolutionary

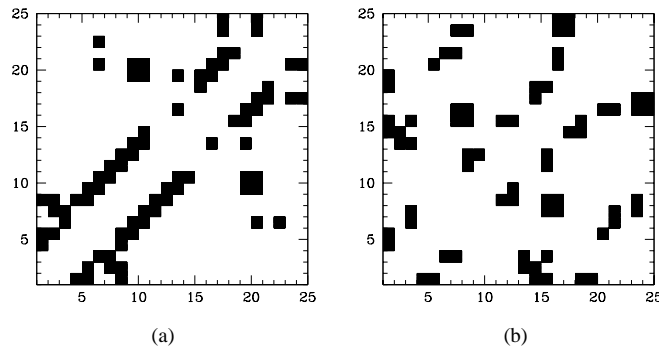


Fig. 7. – The panel on the left [right] shows the contact map of a structure with a very low [average] median folding time. The signature of helices in map (a) is shown by the thick bands parallel to the diagonal, while no such patterns are observed in the matrix (b).

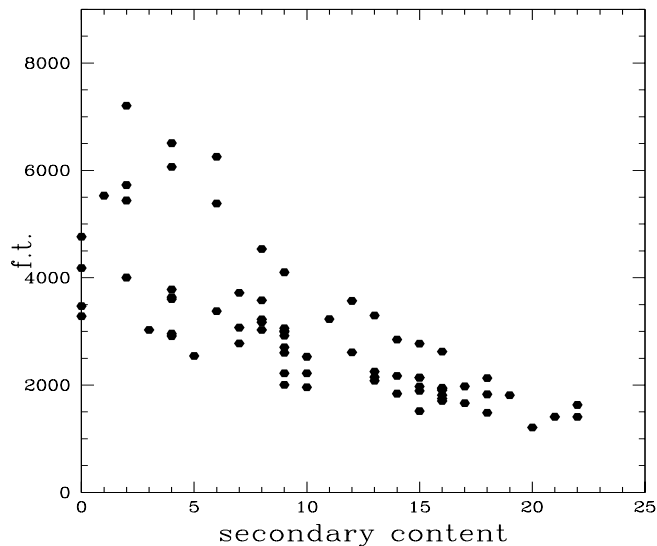


Fig. 8. – Scatter plot of folding time versus secondary content for structures of length 25 collected over several generation of the optimization algorithm.

design of proteins. The results and strategies presented here ought to be applicable in protein-engineering contexts, for example by ensuring optimal dynamical accessibility of the backbone of proteins. A systematic collection of the rapidly-accessible structures of various length should also lead to the creation of unbiased libraries of protein folds.

5. – Density of overlapping conformations for protein structures and role of native state topology in the folding process

The rapid and reversible folding of proteins-like heteropolymers into their thermodynamically stable native state [44] is accompanied by a huge reduction in conformational entropy [45, 46]. Evidence has been accumulating for an achievement of the entropy reduction through a folding funnel favoring the kinetic accessibility of the native state [47, 9, 11, 48, 49]. In Sec. 3 and 4, we have seen that secondary motifs of proteins may arise from the requirements of both being compact and easily kinetically accessible. Here we focus on a further characterization of the special role played by the native structure of proteins; again we will make no use of detailed information regarding amino acid sequences [16]. The study is carried out through a theoretical probe of the conformation space of proteins: a measure of the density of overlapping conformations (DOC) having a given overlap or percentage of contacts in common with a fixed native structure. We show with studies on chymotrypsin inhibitor (reference 2ci2 of the Protein Data Bank) and barnase (1a2p) that the DOC provides key information on the folding pathway. An analysis of the DOC for real protein structures and for artificially generated decoy ones

suggests that an extremal principle is operational in nature, which maximizes the DOC at intermediate overlap, providing a large basin of attraction [13, 50, 9, 11, 48] for the native state and promoting the emergence of secondary structures.

Our study consists of determining the number of structures with a given structural similarity to a putative native state. The structural similarity between the native structure and another one is defined as the percentage of native contacts in the alternative conformation. It is well known that such a measure is a good coordinate characterizing the folding process [36, 51, 33]. To this purpose we adopt the Go scheme introduced in the previous section (see eqn. 1). We also make again use of the FCC coarse-graining to avoid considering as distinct conformations that differ slightly.

The generation of conformations was carried out using a standard Monte Carlo procedure (see e.g. Refs. [33, 53]) which allows one to move simultaneously up to 7 randomly chosen C_α 's to unoccupied FCC sites.

In order to minimize the effects of correlation between successively generated structures, we typically discarded 50 elementary moves before accepting each new conformation. A newly generated conformation was accepted with the usual Metropolis rule according to the change in the Boltzmann weight: $e^{\Delta/K_B T}$, where Δ is the change in contact overlap and T is a fictitious temperature. By choosing T appropriately, one can readily generate conformations with a desired average contact overlap, \bar{q} . At a given temperature, the true number of structures with overlap q is proportional to the number of conformations with overlap q obtained in the simulation multiplied by the Boltzmann weight. On undoing the Boltzmann bias, it is possible to recover the true density of conformations in a region around \bar{q} . In order to obtain the density of conformations for all values of overlap, we performed 2500 Monte Carlo samplings at different decreasing temperatures and then used standard deconvolution procedures [54]. Overall, for each distinct value of the overlap, more than 1000 structures were sampled. We have confirmed that the DOC curves are independent of the starting conformation and that the ‘‘folding’’ DOC obtained starting from a random conformation and cooling agrees to better than 3 % with the ‘‘unfolding’’ DOC obtained starting from the target structure and increasing the temperature.

We begin with the backbones of the chymotrypsin inhibitor and barnase. We generated 2500 structures with a not too large overlap [55] ($\approx 40\%$) for each of them. It turned out that the most frequent contacts shared by the native conformation of 2ci2 with the others involved the helical-residues 30-42 (see top Fig. 9). Contacts involving such residues were shared by 56% of the sampled structures. On the other hand, the rarest contacts pertained to interaction between the helix and β -strands and between the β -strands themselves. A different behaviour (see bottom Fig. 10) was found for barnase, where, again, for overlap of $\approx 40\%$, we find many contacts pertaining to the nearly complete formation of helix 1 (residues 8-18), a partial formation of helix 2, and bonds between residues 26-29 and 29-32 as well as several non-local contacts bridging the β -strands, especially residues 51-55 and 72-75.

Both this picture, and the one described for CI2 are fully consistent with the experimental results obtained by Fersht and co-workers in mutagenesis experiments [57, 58]. In such



Fig. 9. – Ribbon plot (obtained with RASMOL) of 2ci2 (top) and barnase (bottom). The residues involved in the 12 [16] most frequent contacts of alternative structures with overlap $\approx 40\%$ with the native conformations are highlighted in black. The majority of these coincide with contacts that are formed at the early stages of folding.

experiments, the key role of an amino acid at a given site is probed by mutating it and measuring the changes in the folding and equilibrium characteristics. By measuring the change of the folding/unfolding equilibrium constant one can introduce a parameter, termed ϕ -value, which is zero if the mutation is irrelevant to the folding kinetics and 1, if the change in folding propensity mirrors the change in the relative stability of the folded and unfolded states (intermediate values are, of course, possible). Ideally, the measure of the sensitivity to a given site should be measured as a suitable susceptibility to a small perturbation of the same site (or its environment). Unfortunately, this is not easily accomplished experimentally, since substitution by mutation can be rarely regarded as a perturbation. Notwithstanding this difficulty, from the analysis of the ϕ -values obtained by Fersht, a clear picture for the folding stages of CI2 and barnase emerges. In both cases, the crucial regions for both proteins are the same as those identified through the analysis of the DOC reported above. This provides a sound *a posteriori* justification that the main features of the folding of a protein can be followed from a study of the DOC. Remarkably, the method discussed above relies entirely on structure-related properties and suggests that the main features of the folding funnel are determined by the geometry of the “bare” backbone, while the finer details, of course, depend on the specific well-designed sequence. Since our own work [16], other groups have

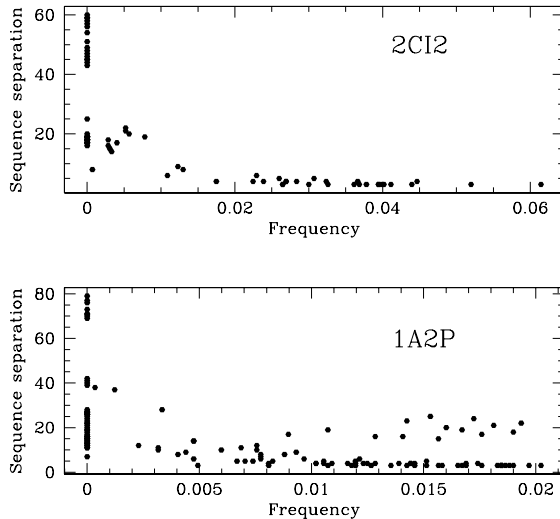


Fig. 10. – Distribution of sequence separation of contacts commonly found in the conformations that overlap with the native state structures of 2ci2 and 1a2p. The most frequent contacts for 2ci2 have a small sequence separation (3-4) and pertain to helix formation. The 1a2p case shows a very different behaviour with several contacts with very large sequence separation.

used similar or alternative techniques to elucidate the role of the native state topology in the folding process [59, 43, 60, 61], confirming the picture outlined here.

Let us consider one way in which proteins, in general, are special and different from arbitrary compact polymers. To do so, we turn to an analysis of three proteins of length 51 (1hcg, 1hja and 1sgp) which have nearly the same number of native contacts (≈ 83). For each structure, we calculated the DOC with the constraint that the total number of contacts in the alternative structures do not exceed the number of contacts in the native state by more than 10 % to avoid excessive compactness. To assess whether the DOC associated with naturally occurring proteins have special features, we generated three decoy conformations of the same length and number of contacts, but with different degrees of short and long range contacts (in sequence separation). These decoys (subject to the aforementioned “physical constraints”) were generated with a simulated annealing procedure to find the structure with the highest overlap with a target contact matrix. By tuning the number of short-range versus long-range entries in the target random contact matrix, we generated three structures with different degrees of compactness and local geometrical regularity.

The logarithmic plots of the DOC are shown in Fig. 11. A striking feature of the curves is that, for intermediate overlap, the DOC of the real proteins is enormously larger than that of the decoys and suggests that naturally occurring conformations have a much larger

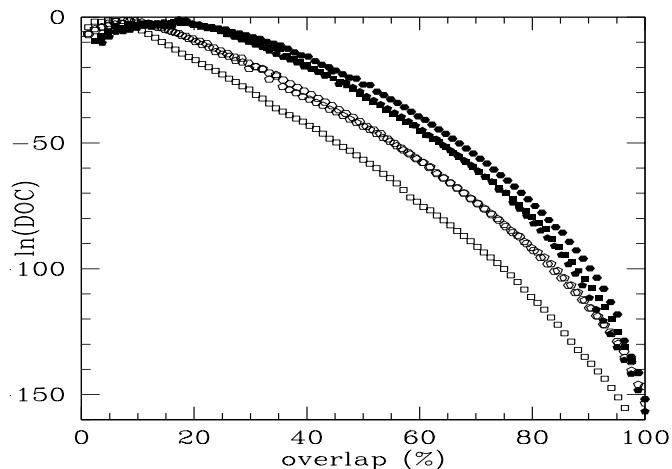


Fig. 11. – Density of overlapping conformations for proteins for 1sgp (filled squares), 1hja (filled pentagons) and 1hcg (filled hexagons). Curves for artificial decoy structures are denoted by the open symbols.

number of entryway structures than random compact conformations. Furthermore, for very high values of the overlap, the steepness of the protein curves is much larger than those of the decoys, showing that the reduction in the conformational entropy is also higher. This implies the existence of a funnel with a very large basin and steep walls. Another significant feature is the good collapse of the protein curves. We verified that this feature also obtains for 1bd0 and 2pk4 which each have 80 residues and 140 and 146 contacts respectively. A simple explanation for the curve collapse, could be that the DOC of real proteins is “extremal”, in that it is close to the maximum possible value for intermediate values of the overlap.

The importance of the locality of contacts for folding kinetics was highlighted recently by Plaxco *et al.* [41] who found a correlation between folding rate and contact order, defined as the average sequence separation of contacts normalized to the total number of contacts and sequence length. With reference to Fig. 11, the contact order values for proteins 1hcg, 1hja and 1sgp are 0.139, 0.214 and 0.204 respectively. For the decoy structures, they are 0.424, 0.222 and 0.179 for the curves denoted by open squares, pentagons and hexagons, respectively. The structure with an unusually high contact order has the lowest DOC curve and optimal sequences designed on it (or equivalently a Go-like model) would be expected to exhibit slow folding dynamics [62] in accord with the findings of Plaxco *et al.* [41].

Secondary structure motifs [34, 15] have characteristic signatures in the contact maps, such as bands parallel to the diagonal (α -helices and parallel β -sheets) or orthogonal to it (antiparallel β -sheets), as it has been shown in the previous section. We have carried out some simple investigations to assess whether a correlation exists between the

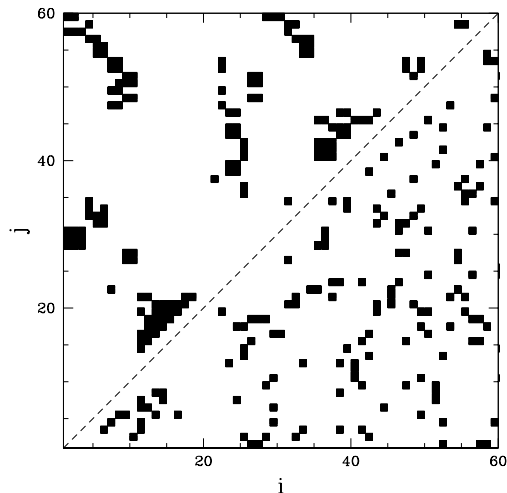


Fig. 12. – The upper [lower] triangle shows a target contact matrix with $L = 60$ that has a large [intermediate] number of contact maps with an overlap of $\bar{q}_{max} - 2$ contacts.

extremality of the DOC curve and the emergence of secondary-structure-like motifs. We considered a space of contact maps [52], within which each of the residues interacted with the same number of other residues, n_c (typically $n_c = 5$, as in the average case of a protein with about 100 residues and a cutoff distance of 6.5 Å). This space contains maps corresponding to both real structures and unphysical ones. Furthermore, to mimic the effects of the rigidity and geometry of the peptide bond, we disallowed contacts between residue i and the four neighboring residues along the sequence $i \pm 2$, $i \pm 1$.

In this context, the maximization of the density of states corresponds to finding the target matrix with the highest number of matrices sharing a given fraction of its contacts. Although it is difficult to solve this problem, for arbitrary values of the overlap, it is relatively easy to generate matrices with an overlap close to the maximum value, \bar{q}_{max} (for a $L \times L$ matrix, $\bar{q}_{max} = L \cdot n_c$). To enumerate all matrices with overlap $\bar{q}_{max} - 2$, one first identifies a pair of non-zero entries in the target matrix \bar{m} : $\bar{m}_{ij} = \bar{m}_{kl} = 1$. Then it is necessary to check whether entries \bar{m}_{il} , \bar{m}_{kj} are both “free” (i.e. equal to zero) and do not correspond to forbidden contacts (e.g. between i and $i + 1$). If this is so, the old pair of entries (and their symmetric counterpart) are set to zero, and the new ones to 1. By considering, in turn, all possible pairs of non-zero entries one can generate all matrices of overlap $\bar{q}_{max} - 2$. Then, by performing a simulated annealing in contact-map space one can isolate the map having the highest number of matrices with overlap $\bar{q}_{max} - 2$.

We carried out our calculations for values of L around 60. The optimal matrices exhibit clustering reminiscent of α -helices and β -sheets, as shown in the upper triangle of Fig. 12. A more quantitative measurement of the secondary-structure content of the optimal matrices can be obtained by considering the correlation functions, $g_{\pm}(x) = \sum_i m_{i, i \pm x}$,

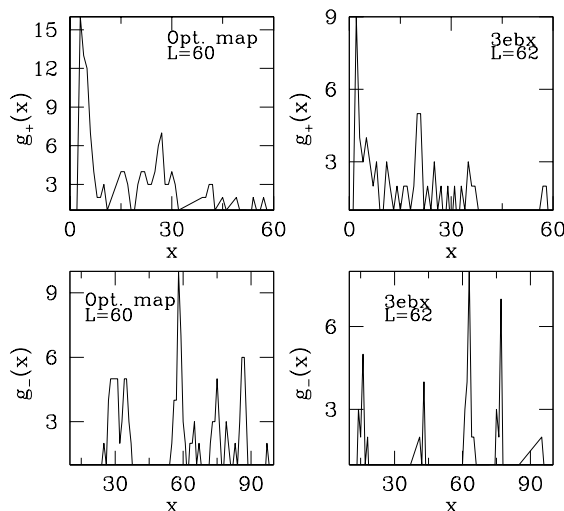


Fig. 13. – Correlation functions (see text) for an optimal target matrix of length 60 and for a protein of length 62 taken from the protein data bank.

which show peaks in correspondence with the sequence separation of residues involved in α -helices and parallel β -sheets (g_+) or antiparallel β -sheets (g_-). A typical plot of the correlation functions for an optimal map of length 60 and for the protein 3ebx (length 62) are shown in Fig. 13. The similarity of the plots is striking, particularly because, in both cases, the height of the peaks in g_+ decreases with sequence separation, unlike the situation with g_- .

In summary, the geometry of protein backbones seems to have been optimized to provide a large basin of attraction to the native state. The results presented here are suggestive of an extremality principle underlying the selection of naturally occurring folds of proteins which, in turn, is shown to be possibly associated with the emergence of secondary structures. This observation complements the one made in the previous section, which highlighted how the presence of secondary motifs boosts the folding kinetics. Strikingly, by examining the DOC associated with a given native structure, it is possible to extract a wealth of information about the sites involved in crucial stages of the folding process. Despite the fact, that such sites are determined from the analysis of their crucial topological role with respect to the native state with no input of the actual protein composition, they correlate very well with the key sites determined experimentally. A striking example is provided in the following subsection, which focuses on an enzyme encoded by the HIV virus. It will be shown that from the mere knowledge of the contact map of the enzyme, one can isolate a handful of hot sites which correlate extremely well the key mutating sites determined in clinical trials of anti-AIDS drugs.

5.1. *Application to HIV-1 protease: drug resistance and folding Pathways.* – A close examination of the curves for the density of states (DOC) can reveal the presence of phase transitions in the system (or more accurately, their analog for finite-size systems). In particular, a change of the concavity/convexity of the DOC curves signals a first-order like transition. This is illustrated in the examples of Figs. 14 and 15 where the curve for the DOC of protein 1hja is shown and accompanied with a graph of the energy versus temperature and the specific heat (obtained through histogram reweighting techniques). Indeed, the peak in the specific heat identifies the folding transition temperature. Naturally, one would like to identify the pairs of sites that contribute most to the C_v peak. For a given pair, (i, j) , this amounts to measuring, as a function of the temperature, T , the quantity

$$(4) \quad C_v(i, j) = \frac{1}{T^2} \langle E(i, j) E_{Tot} \rangle - \langle E(i, j) \rangle \langle E_{Tot} \rangle$$

where $E(i, j)$ is the contribution of the pair to the total interaction energy, E_{Tot} . The most crucial residues will then be identified with those with the highest values of $C_v(i, j)$, which are expectedly observed near the folding transition temperature. We have used this strategy to determine successfully the key sites of HIV-1 [66]. Our simulations, at variance with that described earlier, are now carried out in the continuum. As usual, amino acids are represented as effective centroids placed on C_α atoms, while the peptide bond between two consecutive amino acids, $i, i + 1$ at distance $r_{i, i+1}$ is described by the anharmonic potential adopted by Clementi et al. [63], with parameters $a = 20, b = 2000$. The interaction among non-consecutive residues is treated again in Go-like schemes [36] which reward the formation of native contacts with a decrease of the energy scoring function. Each pair of non-consecutive amino acids, i and j , contributes to the energy scoring function by an amount:

$$(5) \quad V_0 \varepsilon_{ij}^N \left[\left(5 \frac{r_{ij}^N}{r_{ij}} \right)^{12} - 6 \left(\frac{r_{ij}^N}{r_{ij}} \right)^{10} \right] + 5V_1 (1 - \varepsilon_{ij}^N) \left(\frac{r_0}{r_{ij}} \right)^{12},$$

where $r_0 = 6.8 \text{ \AA}$, $r_{i,j}^N$ denotes the distance of amino acids i and j in the native structure and ε_{ij}^N is the native contact matrix whose entries are 1 (0) if i and j are (not) in contact in the native conformation. The contact is defined as in the previous section, i.e. two aminoacids are in contact if their distance is less than 6.5 \AA . V_0 and V_1 are constants controlling the strength of interactions ($V_0 = 20, V_1 = 0.05$ in our simulations)

Constant temperature molecular dynamics simulations were carried out where the equations of motion are integrated by a velocity-Verlet algorithm combined with the standard Gaussian isokinetic scheme [64, 66]. Unfolding processes can be studied within the same framework by warming up starting from the native conformation (heat denaturation).

The free-energy, the total specific-heat, C_v , and contributions of the individual contacts to C_v were obtained combining data sampled at different equilibrium temperatures with

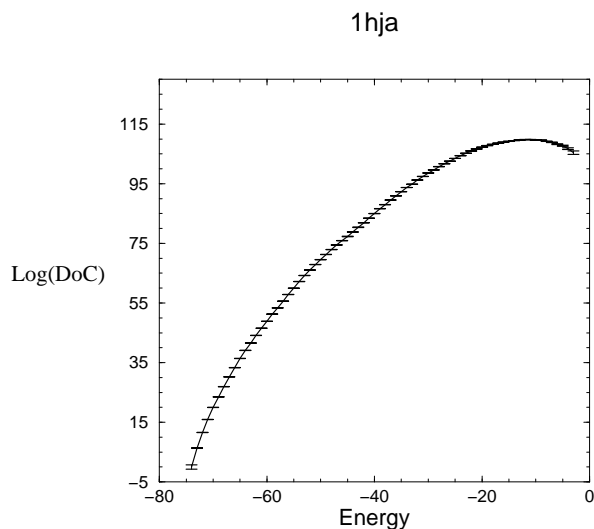


Fig. 14. – Plot of the logarithm of the density of states (density of alternative conformations) versus energy for protein 1hja. The latter is defined as the negative of the number of native contacts present in a given conformation.

multiple histogram techniques [54]. The thermodynamics quantities obtained through such deconvolution procedures did not depend, within the numerical accuracy, on whether unfolding or refolding paths were followed.

The contacts that contribute more to the specific heat peak are identified as the key ones belonging to the folding bottleneck and sites sharing them as the most likely to be sensitive to mutations. Furthermore, by following several individual folding trajectories (by suddenly quenching unfolded conformations below the folding transition temperature, T_{fold}) we ascertained that all such dynamical pathways encountered the same kinetic bottlenecks determined as above.

For the β sheets, the bottlenecks involve amino acids that are typically 3-4 residues away from the turns – specifically, residues 61, 62, 72, 74 for β_3 , 10, 11, 12, 21, 22, 23 for β_1 and 44, 45, 46, 55, 56, 57 for β_2 . At the folding transition temperature, T_{fold} , the formation of contacts around residues 30 and 86 is observed. The largest contribution to the specific heat peak is observed from contacts 29-86 and 32-76 which are, consequently, identified as the most crucial for the folding/unfolding process.

Such sites are physically located at the active site of HIV-1 PR, which is targeted by anti AIDS drugs[65]. Hence, within the limitations of our simplified approach, we predict that changes in the detailed chemistry at the active site also ruin a key step of the folding process. To counteract the drug action, the virus has to perform some very delicate mutations at the the key sites; within a random mutation scheme this requires many trials (occurring over several months). The time required to synthesize a mutated protein with native-like activity is even longer if the drug attack correlates with several

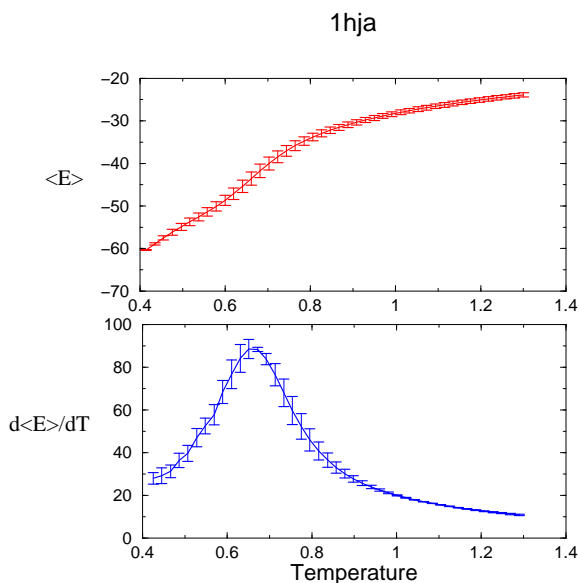


Fig. 15. – Plots of the energy (top) and specific heat (bottom) as a function of temperature for protein 1hja. The curves were obtained through histogram reweighting techniques.

bottlenecks simultaneously.

This is certainly the case for several anti-AIDS drugs. Indeed Table I summarizes the mutations for the FDA approved drugs [67]. In Table II, we list the sites sharing the most important contacts involved in the four bottlenecks TB, β_1 , β_2 and β_3 . Remarkably, among the first 23 most crucial sites predicted by our method, there are 7 sites in common with the 16 distinct mutating sites of Table I. The probability that two sets of 16 and 23 sites randomly taken from a total population of 99 (the length of the HIV-1 PR monomer) share at least 7 sites is only 3 %. Also note that, all the mutation sites of Table I except 82, 35, 36 and 90 fall within a mismatch of at most one position from the sites of Table II. These results highlight the high statistical correlation between our prediction and the evidence accumulated from clinical trials.

In conclusion, the strategy presented here, which is entirely based on the knowledge of the native structure of HIV-1 protease, allows one both to identify the bottlenecks of the folding process and to explain their highly significant match with known mutating residues [66]. This and similar approaches should be readily applicable to identify the kinetic bottlenecks of other viral enzymes of pharmaceutical interest. This could allow a fast development of novel inhibitors targetting the kinetic bottlenecks. This is expected to dramatically enhance the difficulty for the virus to express mutated proteins which still fold efficiently into the same native state with unaltered functionality.

| Name | Point Mutations | Bottlenecks |
|------------------|--|---------------------------------------|
| RTN [68, 69] | 20 , 33, 35, 36, 46 , 54, 63 , 71, 82, 84 , 90 | TB, β_1 , β_2 , β_3 |
| NLF [70] | 30, 46 , 63 , 71, 77, 84 , | TB, β_2 , β_3 |
| IND [71, 72] | 10 , 32 , 46 , 63 , 71, 82, 84 | TB, β_1 , β_2 , β_3 |
| SQV [71, 72, 73] | 10 , 46 , 48, 63 , 71, 82, 84 , 90 | TB, β_1 , β_2 , β_3 |
| APR [74] | 46 , 63 , 82, 84 | TB, β_2 , β_3 |

TABLE I. – *Mutations in the protease associated with FDA-approved drug resistance [67]. Sites highlighted in boldface are those involved in the folding bottlenecks as predicted by our approach. β_i refers to the bottleneck associated with the formation of the i -th β -sheet, whereas TB refers to the bottleneck occurring at the folding transition temperature T_{fold} (see next Table).*

6. – Application of geometrical models to investigate the folding of membrane proteins

While the behavior of small water soluble globular proteins is reasonably well understood [75, 76], much less is known about proteins (membrane proteins: MP) [77, 78, 79, 80, 81, 82, 83, 84, 85, 86, 87, 88] that cross biological membranes and that control solute transport, signal transmission and energy conversion between the two sides of the membrane. This lack of knowledge is related to the difficulty in experimental handling. Membranes consist of phospholipid bilayers with a hydrophobic interior: the surface of MP that interact with such an apolar environment is also hydrophobic and this property causes MP to aggregate in aqueous solution, unless detergents are used. This circumstance makes crystallization of MP's difficult and native structures have been determined only for a handful of them.

Transmembrane proteins (TMP) are the most important and best studied class of MP [77, 78, 89]. They are characterized by the presence of long segments (20 – 30) of amino acids with a high degree of hydrophobicity. In the native structure, these correspond to the transmembrane segments which are inserted in the lipidic interior of the membrane [90]. These segments are predominantly made up of α -helices and β -sheets. The stability

| Bottleneck | Key sites |
|------------|------------------------|
| TB | 22, 29, 32, 76, 84, 86 |
| β_1 | 10,11,13,20,21,23 |
| β_2 | 44,45,46,55,56,57 |
| β_3 | 61,62,63,72,74 |

TABLE II. – *Key sites for the four bottlenecks. For each bottleneck, only the sites in the top three pairs of contacts have been reported.*

of α -helices and β -sheets inside the membrane follow from the formation of hydrogen bonds between the backbone atoms – other possibilities are excluded within the apolar environment [77, 81].

A detailed study of TMP has not yet been possible because little is known about the amino-acids interactions among themselves, with the solvent and in particular with the lipidic interior of the membrane. Here [91], we present a simple strategy to decipher the folding kinetics of transmembrane proteins which is directly inspired by the geometrical approaches we have previously applied to globular proteins. This approach by-passes the details of the complex interactions of the protein in the lipid environment by introducing effective potentials, induced by the presence of the membrane and the associated interface region, that stabilize the native state structure.

Due to the small number of degrees of freedom involved in our scheme, the dynamics of the system can be simulated for the full folding process. Moreover, the free energies of the most relevant intermediate states and free energy profiles along the reaction paths connecting them can be explicitly calculated by thermodynamic integration. Thus the model is able to quantitatively discriminate between the possible reaction paths envisaged for the insertion process of TMP across the membrane [77].

The TMP we considered is made up with the first 66 amino acids (each one represented by a fictitious residue located at the position of the C_α atom) of the first two α -helices of bacteriorhodopsin (Fig. 16a). It has been shown that the first two helices of bacteriorhodopsin can be considered as independent folding domains [92] and that the side-by-side interactions between transmembrane helices play a key role in the stabilization of the protein structure [93]. The membrane is described simply by a slab of width $w = z_{\max} - z_{\min} = 26 \text{ \AA}$. Two non-bonded residues (i, j) are considered to form a contact if their distance is less than 6.5 \AA . In the study of globular proteins, the topology of the native state is encoded in the contact map by considering all the pairs (i, j) of non-consecutive residues that are in contact. Here, in addition, the locations of such pairs with respect to the membrane has to be taken into account. The contacts are divided into three classes:

- *membrane contacts* where both i and j residues are inside the membrane;
- *interface contacts* with i and j in the interface region [77] outside the membrane;
- *surface contacts* with one residue inside the membrane and the other outside.

Thus a given protein conformation can have a native contact but improperly placed with respect to the membrane (*misplaced native contact*). The crucial interaction potential between non-bonded residues (i, j) is taken to be a modified Lennard-Jones 12-10 potential:

$$(6) \quad \Gamma(i, j) \left[5 \left(\frac{r_{ij}^N}{r_{ij}} \right)^{12} - 6 \left(\frac{r_{ij}^N}{r_{ij}} \right)^{10} \right] + 5 \Gamma_1(i, j) \left(\frac{r_{ij}^N}{r_{ij}} \right)^{12} .$$

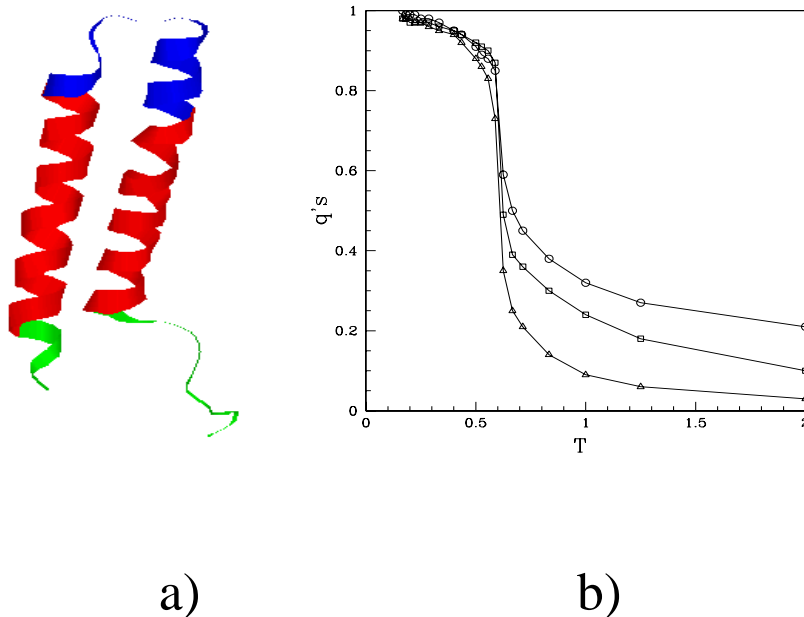


Fig. 16. – Structure and thermodynamics of the helical transmembrane protein. **a)** Ribbon representation of the two-helix fragment of bacteriorhodopsin formed by the first 66 amino-acids. The part inside the membrane is shown in red, the part above (below) the membrane in blue (green). **b)** Average equilibrium fraction of native contacts outside, q_b (\circ), inside, q_m (square), and across, q_s (\triangle), the membrane as a function of the temperature T . All these quantities are expressed in energy unit of ϵ .

r_{ij} and r_{ij}^N are the distance between the residues (i, j) and their distance in the native configuration, respectively. The matrices $\Gamma(i, j)$ and $\Gamma_1(i, j)$ encode the topology of the TMP in the following way: if (i, j) is not a contact in the native state $\Gamma(i, j) = 0, \Gamma_1(i, j) = 1$; if (i, j) is a contact in the native state but not at the proper location (i.e. a misplaced contact) $\Gamma(i, j) = \epsilon_1, \Gamma_1(i, j) = 0$; if (i, j) is a native state contact in the proper region $\Gamma(i, j) = \epsilon, \Gamma_1(i, j) = 0$. This model is intended to describe the folding process in the interface and in the membrane region. Our interaction potential (similar in spirit to the Go model[36] introduced before) assigns two values to the energy associated with the formation of a native contact, ϵ and ϵ_1 . The model captures the tendency to form native contacts. In addition, in order to account for the effective interactions between the membrane and the protein, the model assigns a lower energy, $-\epsilon$, to the contact which occurs in the same region as in the native state structure compared to $-\epsilon_1$ when the contact is formed but in the wrong environment. This mechanism proves to be crucial in driving the insertion of the protein across the membrane.

When $\epsilon = \epsilon_1$, the protein does not recognize the presence of the interface-membrane region and the full rotational symmetry is restored. The difference in the parameters

$(\epsilon - \epsilon_1)$ determine the amount of tertiary structure formation outside the membrane. Our results are independent of the precise values of the energy parameters ϵ and ϵ_1 ($\epsilon > \epsilon_1$) as long as they are not too close to each other.

Our simulations have been performed with $\epsilon_1 = 0.1$ and $\epsilon = 1$. In order to account for the chirality of the TMP, a potential for the pseudodihedral angle α_i between the C_α atoms in a helix corresponding to four successive locations is added which biases the helices to be in their native state structure.

The thermodynamics and the kinetics of the model were studied by a Monte Carlo method for polymer chains carried out in the continuum. The efficiency of the program (usually low for continuum calculations) has been increased by full use of the link cell technique [94] and by the multiple Markov chain method, a new sampling scheme, which has been proven to be particularly efficient in exploring the low temperature phase diagram for polymers [95]. In our simulation 20 different temperatures (measured in dimensionless units) ranging from $T = 2$ to $T = 0.17$ have been studied.

The free energy difference $\mathcal{F}_B - \mathcal{F}_A$ between two states A and B has been estimated as the reversible work that has to be done in order to go from A to B [91]. The free energy differences obtained with this method are accurate to within $\sim 0.1 T_C$ for the various states whereas the free energy barriers are accurate within $\sim 0.5 T_C$. This error takes into account possible hysteresis effects due to the finite simulation time.

The structural similarity between the system equilibrated at temperature T and the native state is shown in Figure 16b in terms of the average fraction of native state contacts as a function of T and partitioned depending on their positions with respect to the membrane. The three curves correspond respectively to the average fraction of native contacts inside (q_m), outside (q_b) and across (q_s) the membrane. All these curves, well separated at high T, collapse for T below the transition temperature $T_C \sim 0.6$, indicating a cooperative effect in the folding. On monitoring the free energy as a function of the energy around T_C , one observes additional local minima (besides those corresponding to the unfolded and folded states) suggesting the presence of an intermediate.

The intermediate is characterized by having the two helices almost completely formed but not yet correctly inserted across the membrane. The presence of these extra minima suggests that non-constitutive membrane proteins would fold with multi-state kinetics corresponding to on-pathway intermediates. To establish the nature of the dominant folding pathway, we have performed a detailed analysis of the folding kinetics. Each independent kinetic folding simulation was started with the equilibrated denatured state at $T^* = 2.5$. The protein is placed initially outside the membrane in the interface region [77], at a distance comparable to the average size of the denatured protein and then suddenly quenched to a temperature ($T = 0.4$) well below the transition temperature. This case simulates the folding kinetics of non-constitutive membrane proteins, i.e. proteins that do not need a translocon providing a 'tunnel' through which the protein is injected into the lipid bilayer. Folding to the native state occurs mainly through the states depicted in Figure 17a with the dominant pathways shown in Figure 17b.

In all the pathways, the system goes from the unfolded state, U to state HI in which 80% of the secondary structure is formed (see q in Figure 18c) and disposed horizontally

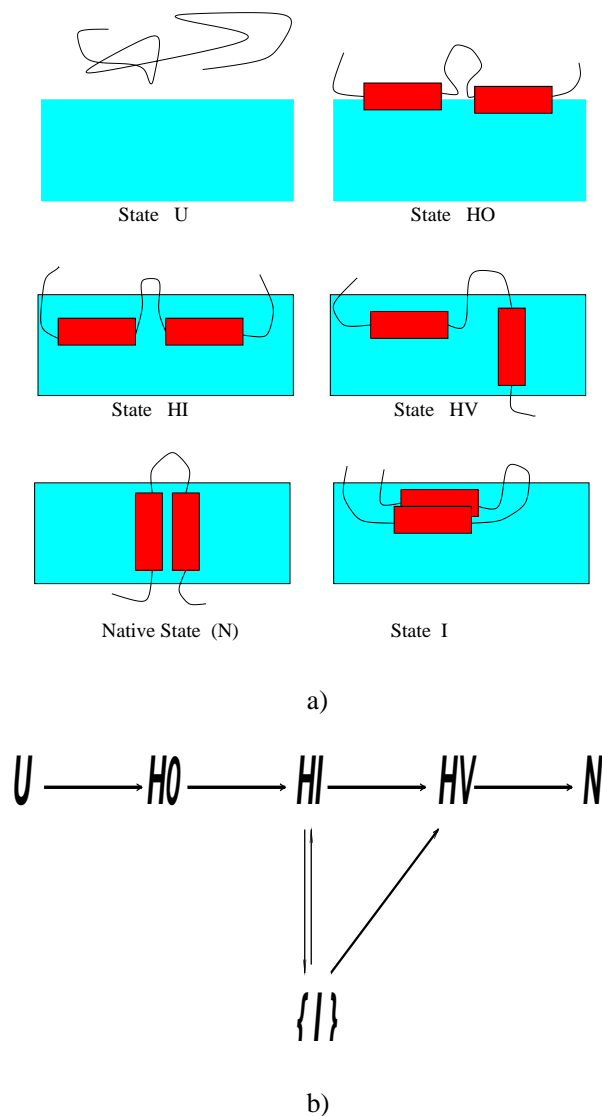


Fig. 17. – Schematic representation of states encountered by our model protein during the folding process. In **a)** the red cylinders denote α -helices that reside within the membrane in the native state. The region inside the membrane is in turquoise whereas the rest represents the interface region [77]. State U denotes the denatured state of the protein, HO is a state in which the helices have been formed but are not yet inside the membrane whereas HI corresponds to a similar state but with the helices completely embedded in the membrane without any inter-helical contacts. HV denotes an obligatory intermediate and N depicts the native state. The state $\{I\}$ represents an ensemble of long lived conformations in which helices are formed inside the membrane with several inter-helical contacts, but with the two α -helices still incorrectly positioned. In **b)** the schematic pathways to the native state are shown.

along the interface. The free energy of this state (measured with respect to the free energy of the fully folded state) is $\sim 2.4 T_C$. This state corresponds to the formation of around 70 % of the membrane contacts. The average time τ_{HI} to reach state HI is of the order of 500 Monte Carlo steps (see Figures 18; each Monte-Carlo step corresponds to 50000 attempted local deformations.). State HI turns out to be an obligatory on-pathway intermediate of the folding kinetics for non-constitutive MP in agreement with the general argument mentioned above. Once the protein reaches state HI , it undergoes a relatively slow process of self-arrangement in order to insert and assemble the secondary structures across the membrane. This process is the rate-limiting step of the folding process, since it involves the translocation, through the lipidic layer, of a substantial number of hydrophilic residues. Among the possible pathways, starting from HI , the most frequent (60% of the cases) and the fastest turn out to be $U \rightarrow HI \rightarrow HV \rightarrow N$. A quantitative characterization of this dominant pathway is presented in Figures 18 (for a single folding process). The intermediate HV is characterized by having one α helix inserted across the membrane and is reached in an average period corresponding to a significant fraction of the total folding time (see Figure 16). The free energy in this state is $\sim 0.98 T_C$. The free energy barrier between HI and HV is at $\sim 4.31 T_C$ (hence, the rate constant of the transition $HI \rightarrow HV$ is proportional to $k_{HI \rightarrow HV} = \exp(-(4.31 - 2.4)T_C/T)$).

The last part of the folding process corresponds to the insertion of the second helix and the assembly of the two secondary structures into the native state structure. This process lasts approximately one third of the folding time along the pathway $U \rightarrow HI \rightarrow HV \rightarrow N$. The quasistatic free energy barrier between HV and the folded state is $\sim 1.66 T_C$. The rate constant of the transition $HV \rightarrow N$ is, therefore, proportional to $\exp(-(1.66 - 0.98)T_C/T)$. These results are consistent with the time scales observed in the unconstrained folding dynamics. At the end, the protein is completely packed, (q_m saturates to 1 (Figure 18a) and the helices are correctly positioned across the membrane (note the second jump in the z coordinate of the center of mass in Figure 18b).

Much slower dynamics can occur when non-obligatory intermediates are visited by the system. These long lived states ($\{I\}$ in Figure 17a) involve a distribution of misfolded regions that trap the system and are characterized by having most of the inter-helical contacts formed (assembly of the secondary structures) but with the two α -helices still incorrectly positioned. Note, for example, that in states $\{I\}$, only transmembrane contacts and some contacts outside the membrane are misplaced and they account for only a small fraction of the native state energy. For this reason, in the states $\{I\}$, the free energy is $\sim 1.44 T_C$, only slightly higher than the free energy of HV . The folding can proceed from $\{I\}$ either by disentangling the two helices and passing through the obligatory intermediate HV , or by the simultaneous translocation through the membrane of the two helices. These processes, however, entail the crossing of a big free energy barrier ($\sim 5.18 T_C$ for the first process and $6.1 T_C$ for the second) and happen with low probability. Indeed, at sufficiently low temperatures, the loss in energy of the interhelical contacts is not compensated by the gain in the configurational entropy due to the uncoupling of the α -helices. Thus below the folding temperature, I-states act as trapping regions for

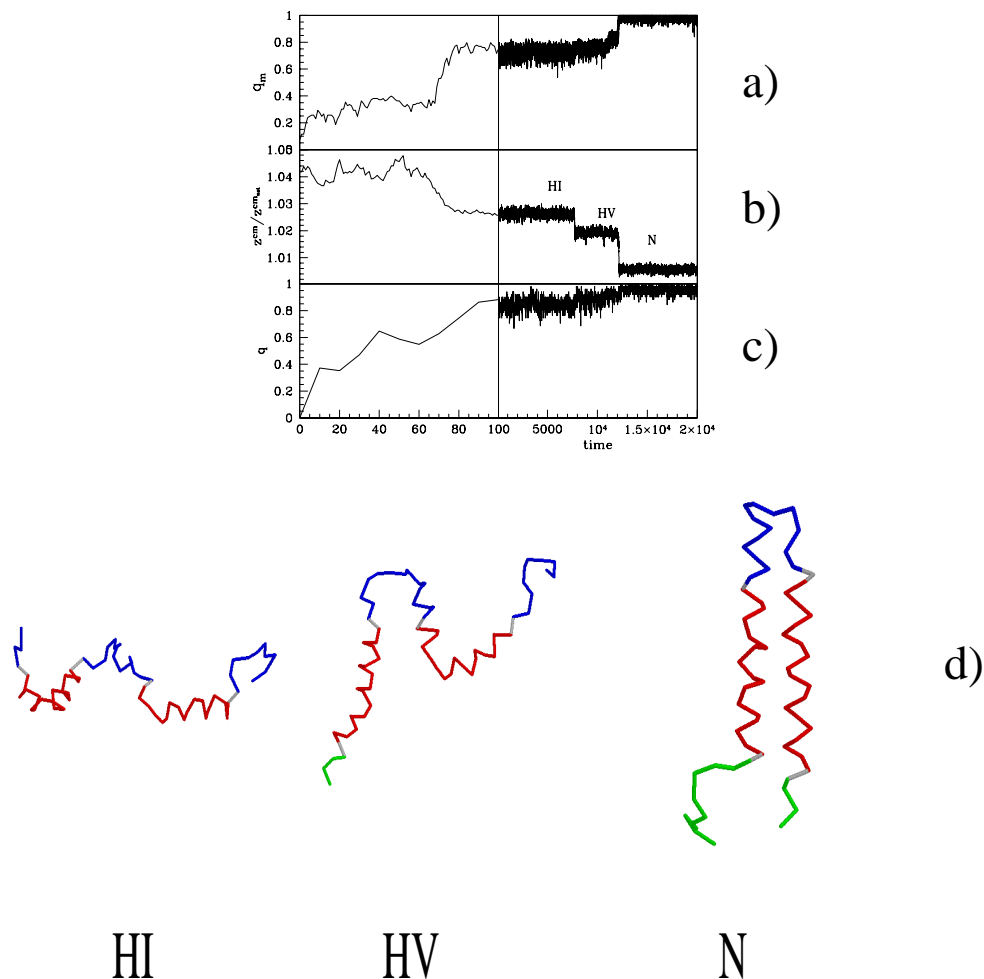


Fig. 18. – Typical time dependence of different parameters as a function of the Monte-Carlo steps for the pathway $U \rightarrow HI \rightarrow HV \rightarrow N$. Fraction of native contacts inside the membrane (a), normalized z-coordinate of the center of mass of the protein (with respect to that of the native state conformation) (b) and overall fraction of native helical contacts (c). (d) Protein conformations at different times during the folding. The colours red, green and blue have the same significance as in Figure 1a with the grey bonds being ones crossing the membrane.

the system and when trapped, the protein spends most of the time during folding in this state.

In summary, we have shown that a topology based model can lead to a vivid picture of the folding process. Our approach predicts a folding process involving multiple pathways with a dominant folding channel. Further details not captured by the present approach may of course change the quantitative nature of the results. However, the model, which

captures the bare essentials of a membrane protein, ought to provide a zeroth order picture of the folding process. Also, as experimental data becomes available, the results could be benchmarked with models of this type to determine the nature of the other factors that matter.

REFERENCES

- [1] Pauling L., Corey R. B. and Branson H. R., *Proc. Nat. Acad. Sci.* **37**, 205 (1951).
- [2] Zimm B.H. and Bragg J., *J. Chem. Phys.* **31**, 526 (1959); Ptitsyn O. B. and Skvortsov A. M., *Biophys.* **10**, 1007 (1965); Lifshitz I. M., Grosberg A.Y. and Khokhlov A. R., *Rev. Mod. Phys.* **50**, 683 (1978).
- [3] Hunt N. G., Gregoret L. M. and Cohen F. E., *J. Mol. Biol.* **241**, 214 (1994).
- [4] Aurora R., Creamer T. P., Srinivasan R. and Rose G. D. *J. Mol. Biol.* **272**, 1413 (1997).
- [5] Nelson J. C., Saven J. G., Moore J. S. and Wolynes P. G., *Science* **277**, 1793 (1997).
- [6] Yee D. P., Chan H. S., Havel T. F. and Dill K. A. *J. Mol. Biol.* **241**, 557 (1994).
- [7] Socci N. D., Bialek W. S. and Onuchic J. N. *Phys. Rev. E* **49**, 3440 (1994).
- [8] Halperin A. and Goldbart P. M., *Phys. Rev. E*, in press (cond-mat/9905306).
- [9] Bryngelson J. D. and Wolynes P. G. *Proc. Nat. Acad. Sci. USA* **84**, 7524 (1987).
- [10] Onuchic J. N., Luthey Schulten Z. and Wolynes P. G. *Ann. Rev. Phys. Chem.* **48**, 545 (1997).
- [11] Leopold P. E., Montal M. and Onuchic J. N., *Proc. Natl. Acad. Sci. USA* **89**, 8721 (1992).
- [12] Wolynes P.G. , Onuchic J. N. and Thirumalai D. , *Science* **267**, 1619 (1995).
- [13] Dill K. A. and Chan H. S., *Nature Structural Biology* **4**, 10- (1997).
- [14] Buchler N. E. G. and Goldstein R. A., *Proteins: Struc. Funct. Genet.* **34**, 113 (1999); Micheletti C., Maritan A., Banavar J. and Seno F. *Phys. Rev. Lett.* **80**, 5683 (1998); Micheletti C. , Maritan A. and Banavar J. , *J. Chem. Phys.* **110**, 9730 (1999).
- [15] Li H., Helling R. , Tang C. and Wingreen N. *Science* **273**, 666 (1996)
- [16] Micheletti C., Banavar J. , Maritan A. and Seno F. *Phys. Rev. Lett.* **82**, 3372 (1999).
- [17] *Nature Structural Biology: Editorial* **6**, 1-2 (1999).
- [18] Sloane N. J. A. *Nature* **395**, 435 (1998).
- [19] Mackenzie D. *Science* **285**, 1339 (1999).
- [20] Woodcock L.V. *Nature* **385**, 141 (1997).
- [21] Car R. *Nature* **385**, 115 (1997).
- [22] Cipra B. *Science* **281**, 1267 (1998).
- [23] Stewart I. *Sci. Am.* **278**, 80 (1998).
- [24] Maritan A., Micheletti C. , Trovato A. and Banavar R., *Nature* **406**, 287 (2000).
- [25] Buck G. and Orloff J. *Topol. Appl.* **61**, 205 (1995).
- [26] Katritch V., Bednar J., Michoud D., Scharein R.G., Dubochet J. and Stasiak A., *Nature* **384**, 142 (1996).
- [27] Katritch V., Olson W. K., Pieranski P., Dubochet J. and Stasiak A. *Nature* **388**, 148 (1997).
- [28] Gonzalez O. and Maddocks J. H. *Proc. Natl. Acad. Sci. USA* **96**, 4769 (1999).
- [29] Buck G., *Nature* **392**, 238 (1998).
- [30] Cantarella J., Kusner R. B. and Sullivan J. M., *Nature* **392**, 237 (1998).
- [31] Rose G. D. and Seltzer J.P. *J. Mol. Biol.* **113**, 153 (1977).
- [32] Maritan A., Micheletti C. and Banavar J. R. *Phys. Rev. Lett.* **84**, 3009 (2000).
- [33] Sali A., Shakhnovich E. and Karplus M. *Nature* **369**, 248 (1994).
- [34] Creighton T. E., *Proteins - Structures and Molecular Properties*, W.H. Freeman and Company, New York (1993), pag. 182-188.
- [35] Levinthal C. *J. Chem. Phys.* **65**, 44 (1968).
- [36] Go N. and Scheraga H.A. *Macromolecules* **9**, 535 (1976).
- [37] Covell D. G. and Jernigan R. *Biochemistry* **29**, 3287 (1990).
- [38] B. H. Park and M. Levitt, *J. Mol. Biol.*, **249**, 493-507 (1995).

- [39] The native state structures of monomeric proteins of length between 50 and 200 show an excellent correlation of this form, when two non-consecutive amino acids along the sequence are defined to be in contact when they are within 6.5 Å of each other.
- [40] Holland J. H., *Adaptation in natural and artificial systems*, MIT press ed. (1992).
- [41] Plaxco K. M., Simons K. L. and Baker D., *J. Mol. Biol.* **277**, 985 (1998).
- [42] Capaldi A. P. and Radford S. E. *Curr. Op. Str. Biol.* **8**, 86 (1998).
- [43] Muñoz V. , Henry E. R., Hofrichter J. and Eaton W. A. *Proc. Natl. Acad. Sci. USA* **95**, 5872 (1998).
- [44] Anfinsen C. *Science* **181**, 223 (1973).
- [45] Karplus M. and Weaver D. L. *Nature* **260**, 404 (1976); *Protein Science* **3** , 650 (1994).
- [46] Ptitsyn O. B., *FEBS Lett* **285**, 176 (1991).
- [47] Chan H. S. and Dill K. A. *Journal of Chemical Physics* **99**, 2116 (1994).
- [48] Onuchic J. N., Wolynes P. G. , Luthey-Schulten Z. and Socci N. D. *Proc. Natl. Acad. Sci. USA* **92**, 3626 (1995).
- [49] Nymeyer H., Garcia A. E. and Onuchic J. N. *Proc. Natl. Acad. Sci. USA* **95**, 5921 (1998).
- [50] Bryngelson J. D., Onuchic J. N., Socci N. D. and Wolynes P. G. *Proteins: Structure, Functions and Genetics* **21**, 167 (1995).
- [51] Camacho C. J. and Thirumalai D. , *Proc. Natl. Acad. Sci. USA* **90**, 6369 (1993).
- [52] Levitt M. *J. Mol. Biol.* **104**, 59 (1976).
- [53] Kolinski A. and Skolnick J. *J. Chem. Phys.* **97**, 9412 (1992).
- [54] Ferrenberg A. M. and Swendsen R. H. *Phys. Rev. Lett.* **63**, 1195 (1989).
- [55] The degree of the overlap may be benchmarked against the typical overlap of any two compact conformations, which is about 10-20 % (consistent with the unfolding simulations of ref. [[56]]). A value of $q \approx 20\%$ thus corresponds to a “molten globule” state.
- [56] Lazaridis T. and Karplus M. *Science* **278**, 1928 (1997).
- [57] Fersht A. R. *Proc. Natl. Acad. Sci. USA* **92**, 10869 (1995).
- [58] Itzhaki L. S., Otzen D. E. and Fersht A. R., *J. Mol. Biol.* **254**, 260 (1995).
- [59] Galzitskaya O. V. and Finkelstein A. V. *Proc. Natl. Acad. Sci. USA* **96**, 11299 (1999).
- [60] Alm E. and Baker D. *Proc. Natl. Acad. Sci. USA* **96**, 11305 (1999).
- [61] Clementi C., Nymeyer H. and Onuchic J. N., *J. Mol. Biol.*, in press (2000).
- [62] Wolynes P. G., *Proc. Natl. Acad. Sci. USA*, **94**, 6170 (1997); Plotkin S., Wang J. and Wolynes P. G., *J. Chem. Phys.* **106**, 1997.
- [63] Clementi C., Carloni P. and Maritan A. *Proc. Natl. Acad. Sci. USA* **96**, 9616 (1999).
- [64] Evans D. J., Hoover W. G., Failor B. H., Moran B., Ladd A. J. C. *Phys. Rev. A* **28**, 1016 (1983).
- [65] Brown A. J., Korber B. T., Condra J. H. *AIDS Res. Hum. Retroviruses* **15**, 247 (1999).
- [66] Cecconi F., Micheletti C., Carloni P. and Maritan A. *Proteins: str. funct and gen.*, **43**, 365-372 (2001).
- [67] Ala P.J, et al. *Biochemistry* **37**, 15042-15049, (1998).
- [68] Molla A. et al. *Nat. Med.* **2**, 760 (1996).
- [69] Markowitz M. et al. *J. Virol.* **69**, 701 (1995).
- [70] Patick A. K., et. al. *Antimicrob. Agents Chemother.* **40**, 292 (1996) .
- [71] Condra J.H. et al. *Nature* **374**, 569 (1995).
- [72] Tisdale M. at al. *Antimicrob. Agents Chemother.* **39**, 1704 (1995).
- [73] Jacobsen H. et al. *J. Infect. Dis.* **173**, 1379 (1996).
- [74] Reddy P. and Ross J. *Formulary* **34**, 567 (1999).
- [75] Fersht A. R., *Structure and Mechanism in Protein Science* W. H. Freeman, New York (1999).
- [76] Karplus M. and Sali A. *Curr. Opin. Struct. Biol.* **5**, 58 (1995).
- [77] White S. H. and Wimley W. C. *Ann. Rev. Biophys. Biomol. Struct.* **28**, 319 (1999).

- [78] Ostermeier C. and Michel H. *Curr. Opin. Struct. Biol.* **7**, 697 (1997).
- [79] von Heijne G. *Prog. Biophys. Molec. Biol.* **66**, 113 (1996).
- [80] Booth P. J. *Folding & Design*, R85 (1997).
- [81] Popot J. L. and Engelman D. M. *Biochemistry* **29**, 4031 (1990).
- [82] Pappu R. V., Marshall G. R. and Ponder J. W. *Nature Structural Biology* **6**, 50 (1999).
- [83] Milik M. and Skolnick J. *Proc. Natl. Acad. Sci. USA* **89**, 9391 (1992).
- [84] Milik M. and Skolnick J. *Proteins: Funct. Stru. Gen.* **15**, 10 (1993).
- [85] Jacobs R. E. and White, S. H. *Biochemistry* **26**, 6127 (1987).
- [86] Roseman M. A. *J. Mol. Biol.* **200**, 513 (1988).
- [87] Wimley S. C. and White S. H. *Designing Transmembrane α -helices That Insert spontaneously* preprint, University of California, Irvine (2000)
- [88] Bonaccini R. and Seno F. *Phys. Rev* **E60**, 7290 (1999).
- [89] Biggin P. C. and Sansom M. S. P. *Biophysical Chemistry* **76**, 161 (1999).
- [90] Deber C. M. and Goto N. K. *Nature Structural Biology* **3**, 815 (1996).
- [91] Orlandini E., Seno F., Banavar J. R., Laio A. and Maritan A. *Deciphering the folding kinetics of transmembrane helical proteins*, preprint (2000).
- [92] Kahn T. W., Sturtevant J.M. and Engelman D.M. *Biochemistry* **31**,8829 (1992).
- [93] Kahn T. W. and Engelman D.M.. *Biochemistry* **31**,6144 (1992)
- [94] Geroff I., Milchev A., Binder, K. and Paul W. *J. Chem. Phys.* **98**, 6256 (1993).
- [95] Tesi M. C., van Rensburg E.J., Orlandini E. and Whittington S. G. *J. Stat. Phys.* **29**, 2451 (1996).
- [96] Sokal A. D., *Nuclear Physics* **B47**, 172 (1996).